

# The evolution of the galaxy B-band rest-frame morphology to $z \sim 2$ : new clues from the K20/GOODS sample

P. Cassata<sup>1\*</sup>, A. Cimatti<sup>2</sup>, A. Franceschini<sup>1</sup>, E. Daddi<sup>5</sup>, E. Pignatelli<sup>3</sup>, G. Fasano<sup>3</sup>, G. Rodighiero<sup>1</sup>, L. Pozzetti<sup>4</sup>, M. Mignoli<sup>4</sup> and A. Renzini<sup>5</sup>

<sup>1</sup>*Dipartimento di Astronomia, Vicolo Osservatorio 2, I-35122, Padova, Italy*

<sup>2</sup>*INAF, Osservatorio Astronomico di Arcetri, Largo E. Fermi 5, I-50125 Firenze, Italy*

<sup>3</sup>*INAF, Osservatorio Astronomico di Padova, Vicolo Osservatorio 2, I-35122, Padova, Italy*

<sup>4</sup>*INAF, Osservatorio Astronomico di Bologna, Via Ranzani 1, I-40124, Bologna, Italy*

<sup>5</sup>*European Southern Observatory, Karl-Schwarzschild-Str. 2, D-85748, Garching, Germany*

## ABSTRACT

We present a detailed analysis of the evolution of the rest-frame B-band morphology of K-selected galaxies with  $0 < z < 2.5$ . This work is based on the K20 spectroscopic sample ( $K_s < 20$ ) located within the Chandra Deep Field South area, coupled with the public deep GOODS HST+ACS multi-band optical imaging available in that field. Thanks to the spectroscopic completeness of this catalog reaching 94%, we can compare the morphological and spectroscopic properties of galaxies with unprecedented detail. Our morphological analysis includes visual inspection and automatic procedures using both parametric (e.g. the Sérsic indices treated by the GALFIT and GASPOT packages) and non-parametric (the Concentration, Asymmetry and clumpiness, CAS) methods. By exploiting the 4-band deep ACS imaging we account in detail for the morphological K-correction as a function of the redshift and show that, while the parametric methods do not efficiently separate early- and late-type galaxies, non-parametric ones prove more efficient and reliable. Our analysis classifies the K20 galaxies as: 60/300 (20%, class 1) normal ellipticals/S0; 14/300 (4%, class 2) perturbed or peculiar ellipticals; 80/300 (27%, class 3) normal spirals; 48/300 (16%, class 4) perturbed or actively star-forming spirals; 98/300 (33%, class 5) irregulars. The morphological and spectroscopic classifications are compatible with each other for more than 90% of the sample galaxies, while 7 class-1 E/S0's show emission lines and 11 spirals and irregulars (class 3+4+5) have purely absorption-line spectra. The evolution of the merging fraction is constrained up to  $z \sim 2$ , by carefully accounting effects of morphological  $k$ -correction: both asymmetry criterion and pair statistic show an increasing merging fraction as a function of the redshift. We finally analyse the redshift-dependence of the effective radii for early- and late-type galaxies and find some mild evidence for a decrease with  $z$  of the early-type galaxy sizes, while disks and irregulars remain constant. Altogether, this analysis of the K20 sample indicates the large predominance of spirals and irregulars at  $0.5 < z < 1.5$  in K-band selected samples at even moderate depths.

**Key words:** galaxies: evolution – galaxies: interactions – galaxies: structure

## 1 INTRODUCTION

Galaxies in the local universe can be organized in a sequence of morphologies (e.g. the Hubble sequence) which must be the result of the specific processes having originated them. Yet, the relative roles over cosmic time of processes such as

merging of dark matter halos, dissipation, starburst, feedback, AGN activity, etc. remain largely conjectural, in particular concerning the establishment of the galaxy morphological differentiation. Therefore, morphological analyses of faint high- $z$  galaxies and studies of the evolution of galaxy sizes with cosmic time give an important insight on how the matter aggregated into the structures that we see today. The combination of a morphological investigation for flux limited

\* E-mail: cassata@pd.astro.it

samples of faint galaxies with complete redshift information provides decisive constraints on the formation epoch and the pattern for the galaxy build-up.

While in the local universe approximately 65% of all galaxies are spirals, 32% are ellipticals and 4% irregulars/peculiars (Marzke et al. 1998), there are indications that in the distant universe the irregular/peculiar fraction becomes predominant (i.e. Glazebrook et al. 1995, Abraham 1996). Van den Bergh et al. (2000, 2001) concluded that most of the galaxies with  $z \gtrsim 0.5$  can be hardly classified within the Hubble scheme: irregular/peculiar/merging objects become more common beyond  $z \sim 0.3$ , spiral structures at  $z \gtrsim 0.6$  are more chaotic than locally and spirals and ellipticals become extremely rare at  $z \gtrsim 1.5$ . Conselice et al. (2004) reached similar conclusions, adding that at  $z \gtrsim 2$  over 80% of the stellar mass is stored in peculiar galaxies.

Exploiting the same data set used in this work Cimatti et al. (2003) investigated the morphology of the K20/CDFS EROs, finding that only the  $\sim 30\%$  of these objects were early-type galaxies.

As a continuation of the K20 survey, Daddi et al. (2004) identified 9 actively star-forming/merging galaxies in the K20/GOODS field with  $1.7 < z < 2.3$  and stellar mass  $M_* > 10^{11} M_\odot$ , while Cimatti et al. (2004) found over the same field 4 passive, early-type galaxies with  $1.6 < z < 1.9$  with similar stellar masses. Thus, while at  $z = 0$  most so massive galaxies are elliptical/S0 galaxies, by  $z \sim 2$  starburst and passive galaxies appear to be in nearly equal numbers.

The Cold Dark Matter (CDM) models of galaxy formation predict that dark matter halos formed by the merging of smaller units in the past. Thus, the evolution of the merging fraction with redshift gives also important cosmogonic information (see for a review Abraham 1998). Several studies report an increasing merging fraction with redshift, both at moderate ( $z < 0.3$ , Patton et al. 1997), and at higher redshifts (Le Fèvre et al. 2000, by pair counts; Conselice et al. 2003, by the Asymmetry measurements).

However, in order to study the evolution with redshift of galaxy morphologies and sizes, the dependence of morphological properties on the wave-band and the effects of the changing rest-frame wavelength as a function of redshift (the so-called morphological  $K$ -correction) have to be taken into account. Galaxies observed in their blue rest-frame appear with later-type morphologies than observed in the red part of the spectrum (e.g. Windhorst et. al 2002; Papovich et al. 2003).

The problem of quantifying morphological properties of high redshift galaxies is still quite open. In the literature, parametric and non-parametric methods are usually applied. The former attempt to model the light distributions with a combination of analytic laws, like de Vaucouleurs or exponential profiles, or the Sérsic model (GALFIT, Peng et al. 2002 and GIM2D, Simard et al. 2002). Various parameters (i.e. bulge/disk B/D ratios or Sérsic indices) are then derived, which are known to correlate with qualitative Hubble classifications. This approach suffers however a number of problems. It needs to assume that the galaxy light distribution is well reproduced by a symmetric profile, hence is not suitable to treat merging structures, spiral arms, dust lanes and so on. Moreover, there are degeneracies in the solutions for multi-component fits (e.g. needed to retrieve the

B/D ratio), because of the large number of free parameters. This becomes quickly unmanageable at decreasing galaxy brightness and number of galaxy pixels.

An often used representation of galaxy morphological types is the parameter  $n$  associated to the Sérsic profile  $\mu \propto \exp(-1/n)$ , with some clear advantages over multi-component fits (Pignatelli et al. 2004). Unfortunately, there are even local ellipticals with a roughly exponential profile, while only the most luminous and massive objects have  $n \sim 4$  (i.e. Caon et al. 1993). This obviously implies an intrinsic level of degeneracy.

Alternatively, non-parametric approaches to quantitative morphology have been developed in the last few years by several authors. The most used ones are the Concentration (C) parameter (Abraham et al. 1996), that roughly correlates with the Sérsic index and with the B/D ratio, and the Asymmetry (A) parameter (Abraham et al. 1996, Conselice et al. 2000), able in principle to distinguish irregulars or mergers from more symmetric galaxies (E/S0/Sa).

More recently another parameter has been introduced, the clumpiness (S), measuring the degree of “patchiness” of a galaxy (i.e. the light in the high spatial frequencies). The clumpiness is expected to correlate with the star-formation rate (Conselice 2003). The advantage of the non-parametric approach is that no a-priory assumption is made about the distribution of light. Some problems however still remain, like the influence of the noise on the asymmetry and clumpiness measures, or the choice of the spatial scale used to compute clumpiness, that must be adapted to the distance and the size of the object, or again the choice of the center of rotation for the computation of the asymmetry.

One aspect that must be taken in consideration when dealing with a morphological analysis is the degree of human interaction needed to obtain the fitting parameters, both for non-parametric and for parametric procedures, in particular when treating large amounts of data, as those made available by the new Advanced Camera for Surveys on HST (e.g. the GOODS, COSMOS, UDF survey projects to mention a few). The GALFIT tool (Peng et al. 2002), for example, has the advantage to allow masking out bad-pixel zones of the image (e.g. dust lanes or spiral arms), in order to improve the fit. However, this appears unfeasible object by object over very large samples. GASPHOT, an automated tool recently developed by Pignatelli, Fasano and Cassata (2004), fitting the galaxy light-profile with a Sérsic model, has been instead defined to retrieve in fully automatic mode fundamental photometric and morphological parameters (magnitudes, radii, axial ratios, Sérsic indices) for all the objects in a given image.

In this paper we exploit the very deep high resolution imaging recently obtained over the CDFS area with ACS/HST taken in the GOODS/HST treasury program (Giavalisco et al. 2004) to make a careful morphological study of galaxies in the K20 sample within this area. In particular, we have exploited the multi-band coverage provided by HST and the redshift information available for each object to minimize the effects of morphological  $K$ -correction: we have studied each object in the ACS band closer to the B-band rest-frame. We also take advantage of the K-band selection, that collects the light from low-mass stars dominating the baryonic content of galaxies, and thus providing a better mass completeness level. The K-band also allows

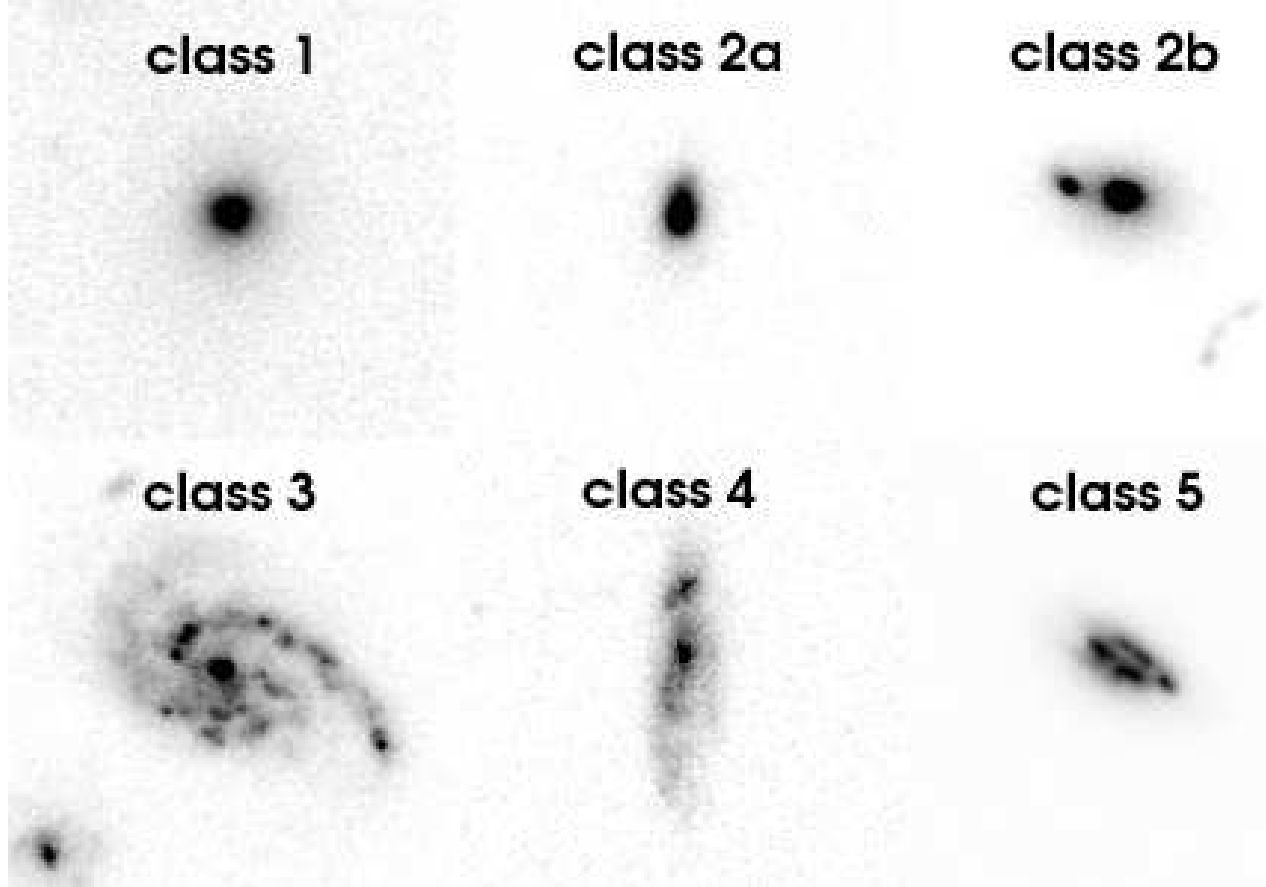


**Figure 1.** Some examples of galaxies representing morphological classes. Each box measures  $4.5'' \times 4.5''$ . From top-left to bottom-right we report: an isolated elliptical (class 1); a perturbed elliptical in which a little distortion of isophotes can be appreciated (class 2a); a couple in which main object is an elliptical (class 2b); a normal spiral (class 3); a peculiar spiral, in which signs of interaction with a little companion at bottom-right can be noted (class 4); an irregular galaxy (class 5).

to minimize the effects of the spectral  $K$ -correction, dust absorption, and evolution.

We are particularly motivated to such an extensive analysis by the excellent optical spectroscopic follow-up obtained for this sample with the ESO Very Large Telescope in the last several years. This paper is devoted to the study of galaxy morphologies and sizes as a function of redshift. A forthcoming paper will expand on statistical analyses of the galaxy distribution as a function of morphology and will attempt to interpret these data with modelistic representations.

The galaxy sample is presented in Sect. 2. The HST/ACS data for the morphological analysis are presented in Sect. 3. In Sect. 4 we use parametric and non-parametric analyses, in particular with GASPHOT and GALFIT and the Concentration-Asymmetry-Clumpiness set, and compare their results with those of a visual inspection. In Sect. 5 we discuss the evolution with the redshift of the inferred fractions of each morphological class, including the merging fraction. The high level of spectroscopic coverage ( $\sim 95\%$ ) is exploited for comparison with the morphological classification in Sect. 6, while our constraints on the redshift evolution of sizes for various morphological types are reported in Sect. 7. Our conclusion are drawn in Sect. 8.

## 2 THE SAMPLE

The original sample was selected in the K-band by the K20 team into two independent sky regions, one centered in the Chandra Deep Field South (CDFS) covering  $32.2 \text{ arcmin}^2$ , the second centered around the QSO 0055-269, and covers  $19.8 \text{ arcmin}^2$ . Detailed informations can be found in Cimatti et al. (2002).

The complete sample consists of 546 objects (including a few stars) down to  $K = 20$ . In this work, we restrict ourselves to the 346 objects lying in the CDFS area, for which high resolution imaging by ACS/HST has recently become available as a result of the GOODS HST Treasury program (Giavalisco et al. 2004). After rejecting stars and quasars, our final sample includes 300 galaxies.

The available data include deep spectroscopy obtained with VLT+FORS1 and VLT+FORS2, and has been recently complemented with ESO/GOODS public data. In the CDFS area the spectroscopic coverage is 92% with K20 data only, and it reaches the 94% including spectra by the ESO/GOODS public spectroscopic survey (Vanzella et al. 2004). For the remaining objects we used throughout the paper the photometric redshifts derived using the ESO/GOODS VLT+FORS1  $BVIRz$  and VLT+ISAAC  $JHK_s$  public imaging (see Cimatti et al. 2002a).

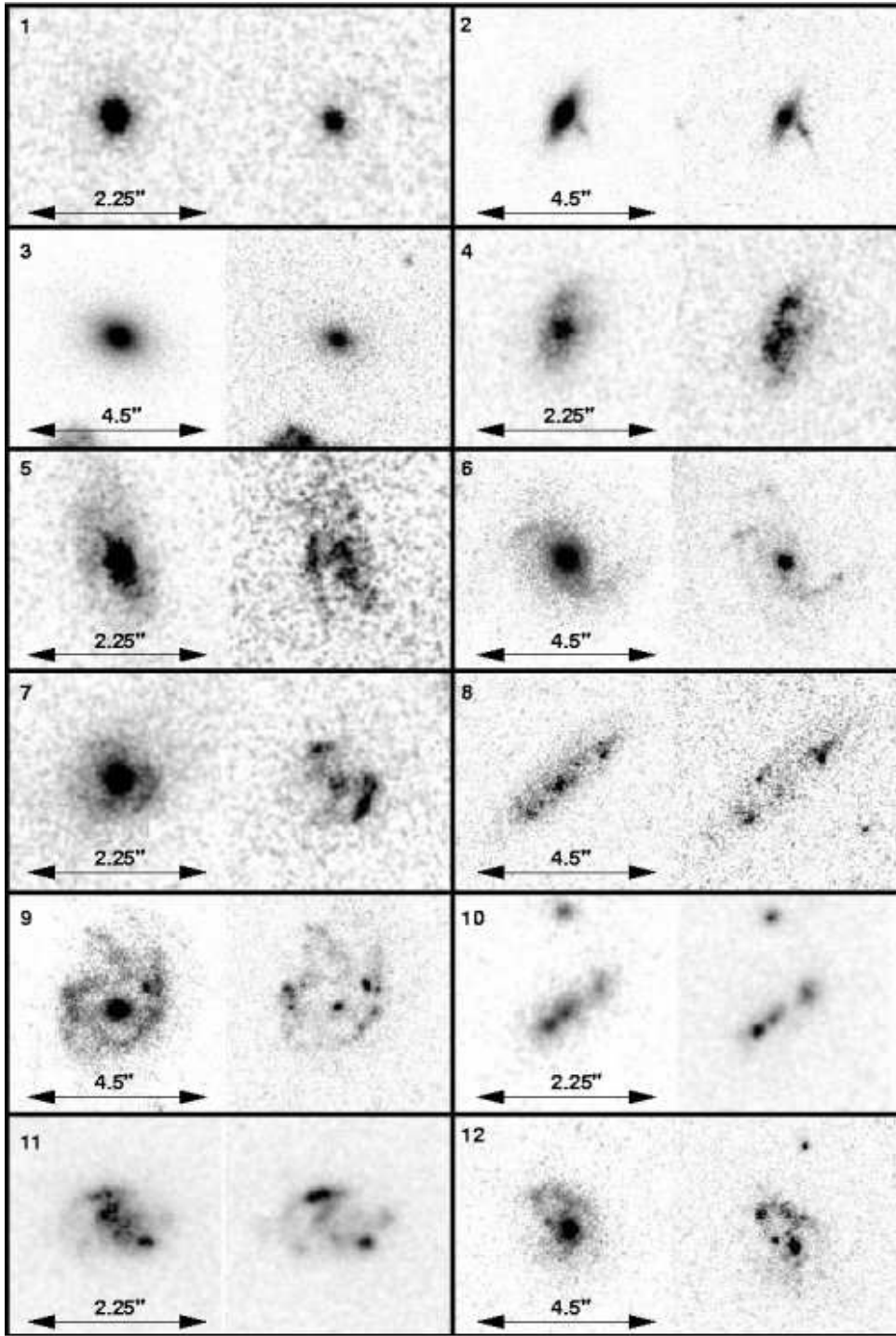


**Figure 2.** A sample of galaxies with  $z \sim 1$  are shown in their z-band, corresponding to  $\sim 4500 \text{ \AA}$  rest-frame (left side of each panel), and in their V-band, corresponding to  $\sim 3000 \text{ \AA}$  (right side of each panel). These examples are representative of morphological the  $K$ -correction problem affecting galaxies observed in their U-band (that is galaxies having  $z \gtrsim 1.5$  observed in z-band) rather than in their B-band rest-frame. The panels labelled with 1, 2 and 3 contains elliptical/S0 galaxies, panels with 4, 5 and 6 normal spirals, panels with 7, 8 and 9 perturbed spirals and panels with 10, 11 and 12 irregular/merger galaxies. The size in arcsec of the images is reported in each panel.

The sample includes objects belonging to two clusters at  $0.665 < z < 0.672$  and  $0.732 < z < 0.740$  (see Cimatti et al. 2002b), including respectively 14 and 32 galaxies.

Galaxy spectra have been automatically classified according to their features into three main classes by Mignoli et al. (2004): 1. early type; 2. early type + emission lines; 3. pure emission line.

### 3 THE HST/ACS DATA

Ground based photometry and spectroscopy was complemented with ACS imaging in the  $BViz$  bands taken in the *GOODS/HST* Treasury Program (Giavalisco et al. 2003). We used the released version 1.0 of the images. The GOODS ACS/HST Treasury Program has surveyed two separate fields (the Chandra Deep Field South and the Hubble Deep Field North) with four broad band filters: F435W (B), F606W(V), F775W(i) and F850LP(z). Observations in the V, i and z filters have been split into 5 epochs, separated by about 45 days, in order to detect transient objects. Observations in the B band are taken during epoch 1 for both fields. Images taken at consecutive epochs have position angles increasing of 45 degrees. Total exposure times are 2.5, 2.5, 5 orbits in the V, i and z bands respectively. The exposure time in the B-band is 3 orbits. In August 2003 the GOODS team released the version 1.0 of the reduced, stacked and mosaiced images for all the data acquired during the five epochs of observation. To improve the PSF sampling, the original images, which have a scale of 0.05 arcsec/pixel, have been drizzled onto images with a scale of 0.03 arcsec/pixel.

We have exploited the multi-band high resolution imaging to study each objects in the ACS band closer to the B rest-frame, in order to minimize effects of morphological  $K$ -correction: the F435W filter is used in the range  $0 < z < 0.2$ , F606W in the range  $0.2 < z < 0.55$ , F775W in the range  $0.55 < z < 0.85$  and F850LP for  $z > 0.85$ . The z band is only a poor approximation of the B-band rest-frame for objects with  $z \gtrsim 1.2$ , approaching towards to the U-band rest-frame. We will come back later to this problem.

### 4 DATA ANALYSIS

The morphological analysis has been performed in three steps: (a) a visual inspection, in order to assign each object to morphological classes based on the detected features (spiral arms, tails, double nuclei...); (b) a surface-brightness profile analysis performed with GASPHOT and GALFIT, in order to quantify morphology and in particular to extract Sérsic indices; (c) a non-parametric analysis of the distribution of the galaxy light, using the measures of asymmetry, concentration and clumpiness (or smoothness) to separate different galaxy types. In the following we will use only the results obtained by the visual inspection, reinforced by those from automatic procedures. However, we are also interested in identifying a completely automatic procedure able to segregate at least early- from late-type galaxies with a low level of interaction. This procedure will be useful for the incoming new very large and deep surveys like GOODS and COSMOS.

### 4.1 Visual inspection and morphological classification

The galaxies have been separated into five morphological classes (see Fig.1): 1. Early-type galaxies (ellipticals and S0); 2. Peculiar early-types, that is either spheroidals objects showing some amount of isophotal asymmetry, or galaxy pairs in which the main component is clearly elliptical; 3. Normal Spirals with regular disk structure and no evidence for luminous high-star formation regions; this kind of galaxies have usually a luminous dominant bulge; 4. Perturbed Spirals, that is disk-dominated galaxies (with a central bulge) showing an asymmetric structure due to interactions or to zones of strongly enhanced star formation; 5. Irregular galaxies, that is objects with a high degree of asymmetry showing no evidence for a disk component.

Figure 1 illustrates some galaxies extracted from the 5 morphological classes.

The visual inspection has been performed independently by three authors, PC, GR and GF, in order to minimize systematic trends. For the cases on which the classifications did not match, we have chosen the median morphological value.

Eventually, we have assigned 60 objects to class 1, 14 to class 2, 80 to class 3, 48 to class 4 and 98 to class 5. The classes with peculiar disks and irregular galaxies are the most populated ( $\sim 50\%$  of the galaxies fall in class 4 or 5). It was not possible to systematically separate ellipticals from S0, given the reduced isophotal area covered by the sources. Among the 46 galaxies belonging to the above mentioned clusters, 20 are normal ellipticals, 3 are peculiar ellipticals, 10 are normal spirals, 5 are peculiar spirals and 8 are irregulars.

#### 4.1.1 The effect of $K$ -correction on the objects with $z > 1.2$

We analyze here the effects of  $K$ -correction on the morphological classification of objects having  $z \gtrsim 1.2$ . The reddest ACS available band (the F850LP filter) does not match for these galaxies the B-band rest-frame, that is used for the morphological analysis of the remaining objects at lower  $z$ , but rather matches the U-band rest-frame.

To this end we have selected a subsample of galaxies with  $z \sim 1$ , and we have compared their morphologies in the V (6060 Å, corresponding to the U-band rest-frame) and z (8500 Å, corresponding to the B-band rest-frame) ACS bands. In particular, 3 Elliptical/S0 galaxies (1 – 3 in Fig. 2), 3 Normal Spirals (4 – 6 in Fig. 2), 3 Perturbed Spirals (7 – 9 in Fig. 2) and 3 Irregulars (10 – 12 are shown as examples in Fig. 2).

*Ellipticals.* The galaxies in panel 1 and 3 have a clear elliptical morphology both in U as in B rest-frame. The galaxy in panel 2 represents a border case: according to its B rest-frame image has been classified as S0 and assigned to class 2; it must be noted that this is the only case in which the classifiers have been able to distinguish S0 from E or Sa morphologies. In the U rest-frame the S0 morphology is roughly preserved, tending perhaps to resemble to a Sa Spiral.

*Normal Spirals.* The galaxies in the panels 4, 5 and 6 have been classified as normal spirals according to the presence

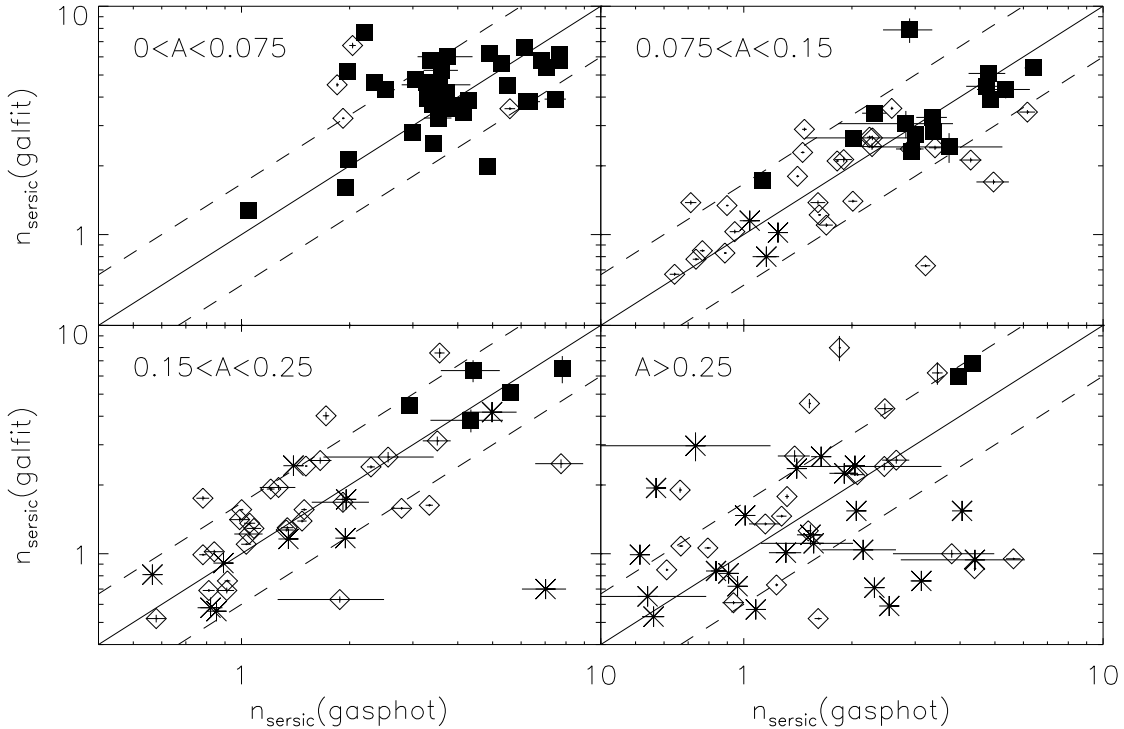


**Figure 3.** Sérsic index retrieved by Gasphot versus those retrieved by Galfit for K20 galaxies in four bins of asymmetries (A). Dashed lines mark the region where  $\Delta n/\bar{n} \leq 0.5$ . Filled squares are visually classified ellipticals/S0 galaxies (class 1 and 2), open diamonds are spirals (class 3 and 4) and crosses are irregulars.

in their B-band rest-frame images of a central bulge on top of a spiral-dominated disk. It turns out that for the objects in panel 4 and 6 the morphology is preserved going from B to U rest-frame; in the remaining case the bulge becomes much less luminous in U and the star formation regions of the disk make the morphology looking more irregular.

*Perturbed Spirals.* The galaxies in the panels 7, 8 and 9 have been classified as spirals according to the presence in their B-band rest-frame of a disk structure with a central bulge (less luminous than in the above case). The peculiarity depends on the presence of asymmetric structures (zones of high star formation or interactions). Also in this case, the U rest-frame luminosity of the central bulge decreases, making the asymmetries more evident. In particular, in two cases (panels 7 and 8) the dominant morphology becomes irregular, whereas perhaps in the latter case (panel 9) the underlying disk structure and the spiral arms structure are preserved.

*Irregulars.* In all the three cases the irregular morphology is preserved, as expected.

Observing the Fig. 2, it turns out that the most impor-

tant effect of the morphological *K*-correction concerns objects with a B rest-frame spiral-like morphology, which may become irregulars in the U rest-frame imaging. In order to quantify the percentage of mis-classified spirals at  $z \gtrsim 1.2$ , we have performed the comparison between B and U rest-frame imaging over a sample of 27 disk galaxies at  $z \sim 1$ . We found that the morphology moved to irregular only in 5/27 cases (18%). Since we do not know if the  $z \sim 1$  galaxies are representative of the universe at higher  $z$ , this result suggests that at  $z \gtrsim 1.2$  the fraction of irregular galaxies could be slightly over-estimated, as the fraction of spirals could be slightly under-estimated.

We have also performed the above analysis over a sample of 10 elliptical galaxies at  $z \sim 1$ , seeking cases similar to panel 2 of Fig. 2. We concluded that the the cited case is the only in which elliptical morphology is not preserved moving from B to U rest-frame. Then the number of elliptical galaxies at  $z > 1.2$  seems to be rather solid.

## 4.2 Surface brightness profile analysis

### 4.2.1 The GASPHOT automatic analysis tool

GASPHOT is a package for fully automatic surface photometry of galaxies, with a very low level of visual interaction, hence particularly suitable for very large imaging datasets (Pignatelli et al. 2004). However, its validity for morphological classification is to be considered only in a statistical sense, rather than on a single object basis.

The tool uses a modified version of SExtractor (Bertin & Arnouts 1996) to identify galaxies in the image and to extract isophotes. Then it analyzes the profiles and derives the main photometric parameters of each identified object. The program determines the light growth-curves along the major and minor axes. These are then fitted with a Sérsic law ( $\mu \propto r^{1/n}$ ), convolved with the PSF, with five free parameters: the total magnitude  $M_{tot}$ , the half-luminosity radius in arcsec  $r_e$ , the Sérsic index  $n$ , the axial ratio  $b/a$  and the value of the local background.

This one-dimensional approach provides a more robust estimate than a more complex 2-D fit of the surface brightness image, which is more sensitive to the presence of features like spiral arms, double nuclei or dust lanes. It is also less affected by instrumental artifacts in the real image, particularly for very faint galaxies like our own.

Profiles with high values of the Sérsic index imply an early-type morphology (the de Vaucouleurs profile has  $n=4$ ), while low values usually indicate later-type morphologies (the exponential profile has  $n=1$ ). Unfortunately, many bulge-dominated objects have intermediate Sérsic indices, or even an exponential profile, so a residual degeneracy still remains in assigning the morphological class.

The situation gets more complicated when treating irregular galaxies and when dealing with blended objects. The isophotes flagged by SExtractor as blended are not used in the fit, in order to minimize distortions. This makes the fitting procedure much more certain. In this framework, irregular galaxies can only be identified by very large  $\chi^2$  or failed fits. In these cases, however, the photometric parameters obtained are obviously meaningless.

### 4.2.2 The automatic analysis package GALFIT

GALFIT is an automatic tool to extract structural parameters from galaxy images. At variance with GASPHOT, GALFIT fits the whole 2-D sky-projected light distribution. It combines together different parametric models (the Nuker law, the Sérsic-de Vaucouleurs profile, the exponential disk, the Gaussian or Moffat functions) and allows multi-component fitting (useful to calculate e.g. Bulge/Total light ratios) and provides measures of the diskyness/boxyness of the examined galaxy. If available, the PSF is used to convolve the model before fitting. It is also possible to mask out of the fit peculiar regions (dust lanes, nearby companions, spiral arms, etc.) that the user wants to exclude.

Even if GALFIT allows to reach a high level of detail in modeling galaxy light, it needs substantially more interaction for each individual object and it works well for bright galaxies with good sampling, rather than for the fainter ones closer to the sensitivity limit.

We have built a tool automatically running GALFIT

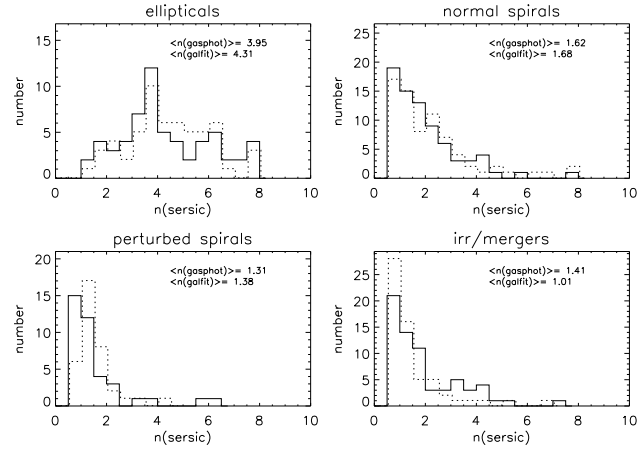


**Figure 4.** The distributions of Sérsic indices retrieved by GASPHOT (continuous line) and GALFIT (dotted line) for the four morphological classes. The mean value of  $n_{Sersic}$  for the two tools is reported in each panel.

over all galaxies of interest, making use of SExtractor to determine the required initial guess of the model parameters (magnitudes, scale radii, axial ratios and position angles).

### 4.2.3 Comparison between GALFIT and GASPHOT

Although GALFIT can in principle use multi-component models, in order to compare with each other the results from GALFIT and GASPHOT, we have forced GALFIT to the single component, Sérsic model.

We must also first clear the sample from the objects for which the two tools were not able to produce a fit. In fact, because of the numerical approximations involved and in order to avoid unrealistic run-away solutions, GASPHOT allows the fitting parameters to move during the fitting process in the region limited by  $R_e > 0.7$  pixels and  $0.5 < n < 8$  only. Solutions whose best fit-parameters are beyond these boundaries are rejected, and the related galaxies are flagged as "failed fits". GALFIT has no such limits: however, in order to perform a consistent comparison between the results of the two tools, we put the same limits on the best-fit parameters of both tools and removed from the sample those for which one of the two tools was not able to find a solution.

In addition, due to the very low S/N ratio, GASPHOT and GALFIT were not able to produce any fit for 16 and 14 galaxies, respectively. Once we removed these objects, mainly irregular or high asymmetric objects, the galaxies left in the sample are respectively 254 (GASPHOT) and 236 (GALFIT), of which 211 are in common.

In Fig. 3 we have reported the Sérsic indices retrieved by GASPHOT against those obtained by GALFIT, finding that 73% of the sample is included in the region  $|n_{GASPHOT} - n_{GALFIT}|/\langle n \rangle \leq 0.5$ , where  $\langle n \rangle$  is the average of the two results, while 9% have  $\Delta n/\langle n \rangle \geq 1$ . It is worth stressing that, even though for toy galaxies the results from GASPHOT and GALFIT have been found to differ less than 10% from one another (Pignatelli et al. 2004), the large scatter in Figure 3 is not surprising when dealing with real featured galaxies, with light distributions often asymmetric and far from being stick to the models. In particular, due to the

different fitting approaches adopted (1D vs. 2D), we expect that GASPHOT and GALFIT provide rather different results at increasing asymmetry. Thus, we split the Figure 3 in different bins of the asymmetry parameter  $A$ . Actually, apart from the first asymmetry bin, the scatter around the 1:1 relation increases with the asymmetry of the galaxies analyzed, and a similar trend is found for the number of failed fits as a function of the asymmetry: more asymmetric galaxies are obviously harder to model with a spherically symmetric Sérsic law. The large scatter observed in the first bin of  $A$  is due to the predominance of early-type galaxies (high values of Sérsic index) and to the fact that the uncertainty of the retrieved values of  $n$  intrinsically increases with the Sérsic index itself (Pignatelli et al. 2004).

A similar trend is visible in Fig. 5, where we show the comparison between the optical radii retrieved by the two tools. Even now 73% of the sample is comprised in the region  $|r_{\text{GASPHOT}} - r_{\text{GALFIT}}|/\langle r \rangle \leq 0.5$ . In this case, however, the scatter around the 1:1 relation is not symmetric: there is a large amount of galaxies for which the GALFIT scale radius is considerably larger than that obtained by GASPHOT. A similar effect was also found by Pignatelli et al. (2004) in a systematic comparison between the two tools.

We checked visually the objects for which this difference was more noticeable. We found that, for compact objects with a small isophotal radius and high Sérsic index, GALFIT can sometimes recover unrealistic optical radii, often many times larger than the isophotal area itself.

Finally, we want to investigate further whether a criterion based on the Sérsic index could be able to separate early- from late-type galaxies. Ravindranath et al. (2004) for example classified as bulge-dominated and disk-dominated galaxies objects with  $n_{\text{Sersic}} \leq 2$  and  $n_{\text{Sersic}} > 2$ , respectively.

In Fig. 4 the distributions of the Sérsic indices obtained by GASPHOT and GALFIT for the five morphological classes are reported (normal E's/S0 and perturbed ellipticals are plotted together). It is worth noticing that, while the results of the two tools for individual objects may differ, the statistical distributions are quite similar.

The number of elliptical/S0 galaxies (morphological class 1 and 2) which have Sérsic indices lower than 2 are only 6 and 3 according to GASPHOT and GALFIT respectively. Instead, the contamination of late type galaxies with Sérsic indices greater than 2 is larger (56/254 and 50/237, according to GASPHOT and GALFIT respectively). From Figure 4 we must conclude that the Sérsic index alone just provides a broad, not univocal indication of the morphological type. Since this index is a measure of the concentration of light, this is in agreement with the results of Abraham et al. (1996), who found that, besides the Concentration, at least one more parameter is needed to classify galaxies.

### 4.3 The CAS parameter set

The non-parametric methods for morphological estimates are those which do not need to assume a parametrized analytic function to model the galaxy light distribution. They constitute an important complement to the problem of quantitative morphology (Abraham et al. 1996, Conselice et al. 2000, Conselice 2003). We use the classical Concentration, Asymmetry and clumpiness (or smoothness) parameters.

The Concentration correlates with the Sérsic index: high Concentration values correspond to early-type morphology, while lower values are suggestive of a disk-dominated or irregular galaxy. The Asymmetry can distinguish irregular galaxies or perturbed spirals from relaxed systems as E/S0 and normal spirals. The Clumpiness quantifies the degree of structure on small scales, and roughly correlates with the rate of star formation.

#### 4.3.1 Definitions

The operational definitions of the three parameters may differ from author to author. We refer to the Conselice et al. (2003) definitions, but we modified them in order to make simpler and faster the computations. The Concentration is a logarithmic ratio of the apertures containing 80% and 20% of the total flux:

$$C = 5 \log \left( \frac{r_{80}}{r_{20}} \right). \quad (1)$$

operatively, we interpolate the flux growth curve obtained using 12 aperture radii within which SExtractor calculates the flux.

The Asymmetry measures how much the galaxy light is symmetric with respect to a rotation of  $180^\circ$  around the galaxy centroid. So the Asymmetry is qualitatively the residual of the difference between the original  $I_0$  and the rotated  $I_{180}$  galaxy image:

$$A = \frac{\sum |I_0 - I_{180}|}{2 \sum |I_0|}. \quad (2)$$

In order to reduce the influence of the background noise, we subtract from the galaxy image the background given by SExtractor, and we remove those pixels having values lower than 1.5 times the  $rms$  of the background. The results strongly depend on the adopted galaxy centroid. We solve this problem by computing the Asymmetry on a grid of  $100 \times 100$  points around the center calculated by SExtractor. The distance between contiguous points in this artificial grid is 0.4 pixels, so the Asymmetry is computed for points up to  $\pm 20$  pixels far from the initial center. The Asymmetry is defined as the minimum of the values computed on the whole grid.

The Clumpiness measures the fraction of galaxy light lying in the high spatial frequencies. It is computed by subtracting from the original an image smoothed by a box of a given size:

$$S = \sum \frac{(I_0 - I_\sigma)}{I_0} \quad (3)$$

where  $I_0$  is the original image and  $I_\sigma$  is that convolved with a box of scale  $\sigma$ . The value of the retrieved clumpiness depends strongly by the scale used for the convolution. We use  $\sigma = 2/3r_{\text{SE}x}$  and  $\sigma = r_{\text{SE}x}$  (where  $r_{\text{SE}x}$  is the FLUX\_RADIUS parameter given by SExtractor) respectively for galaxies with  $r_{\text{SE}x}$  lower and greater than 5 pixels. Again, in order to reduce the influence of the background noise we remove those pixels having values lower than 2 times the  $rms$  of the background.

To automatically compute the CAS parameters for all the galaxies in our image we have used specifically a designed IDL tool which uses SExtractor to produce the flux

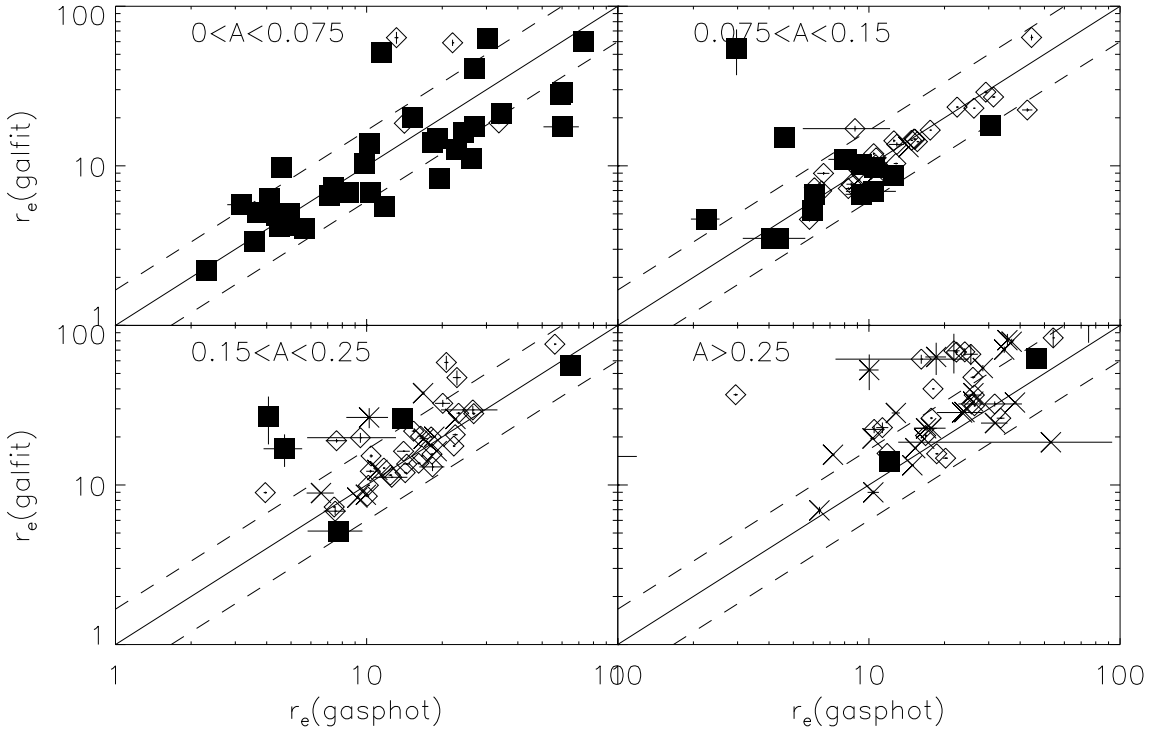


**Figure 5.** Scale radius retrieved by GASPHOT versus those retrieved by GALFIT for K20 galaxies in four bins of asymmetry. Dashed lines mark the region where  $\Delta r_e / r_e \leq 0.5$ . Filled squares are ellipticals/S0 galaxies (class 1 and 2), open diamonds are spirals (class 3 and 4) and crosses are irregulars.

growth curves of galaxies, then IDL calculates the concentration indices, subtracts the background and filter noisy pixels. Finally a postage cut for each galaxy of interest is produced and these postages are suitably rotated and convolved to calculate Asymmetry and Clumpiness.

We compute the CAS parameters in the ACS bands roughly corresponding to the B-band rest frame for each galaxy.

#### 4.3.2 Simulation of CAS parameters for high- $z$ galaxies

The poor sampling of high  $z$  galaxies is likely to affect the measures of the CAS parameters. To check and quantify this point, we have simulated the effects of moving local galaxies with known CAS values to higher redshifts. We have used as test objects all the galaxies in the sample having  $z < 0.3$ . Following Conselice (2003), the angular size of galaxies is reduced by a rebinning factor  $b$  given by the ratios of the angular diameter distances:

$$b = \frac{d_A(z_2)}{d_A(z_1)} \quad (4)$$

where  $z_1$  and  $z_2$  are respectively the initial and final redshifts. Then, pixel fluxes are reduced by the cosmological  $(1+z)^4$  factor and are K-corrected. Operatively, we first filter out the noise of the test galaxies with a simple smoothing algorithm, and, after rebinning, changing the angular sizes and correcting the pixel fluxes, we convolved the images with a model of the PSF. Finally the noise is re-added and the CAS parameters are computed.

In Fig. 6 we report the results of these simulations for 4 ellipticals, 7 spirals (including normal and perturbed spirals) and 11 irregulars galaxies. For comparison, the ranges of values that we measured for the 300 galaxies in our sample are reported as vertical bars. Although the number of simulated objects is not large, we note that the Asymmetry A does not depend on  $z$  for spirals and irregulars, apart from an increase of the scatter at increasing redshift. On the other hand, a small increment of the mean value with  $z$  is present for the ellipticals.

There is a moderate dependence on redshift in the estimate of Concentration C for the ellipticals: values at  $z > 0.5$  are systematically lower than local values. Again, the scatter increases with the redshift for all classes.

As for the Clumpiness S, a bias appears to be introduced

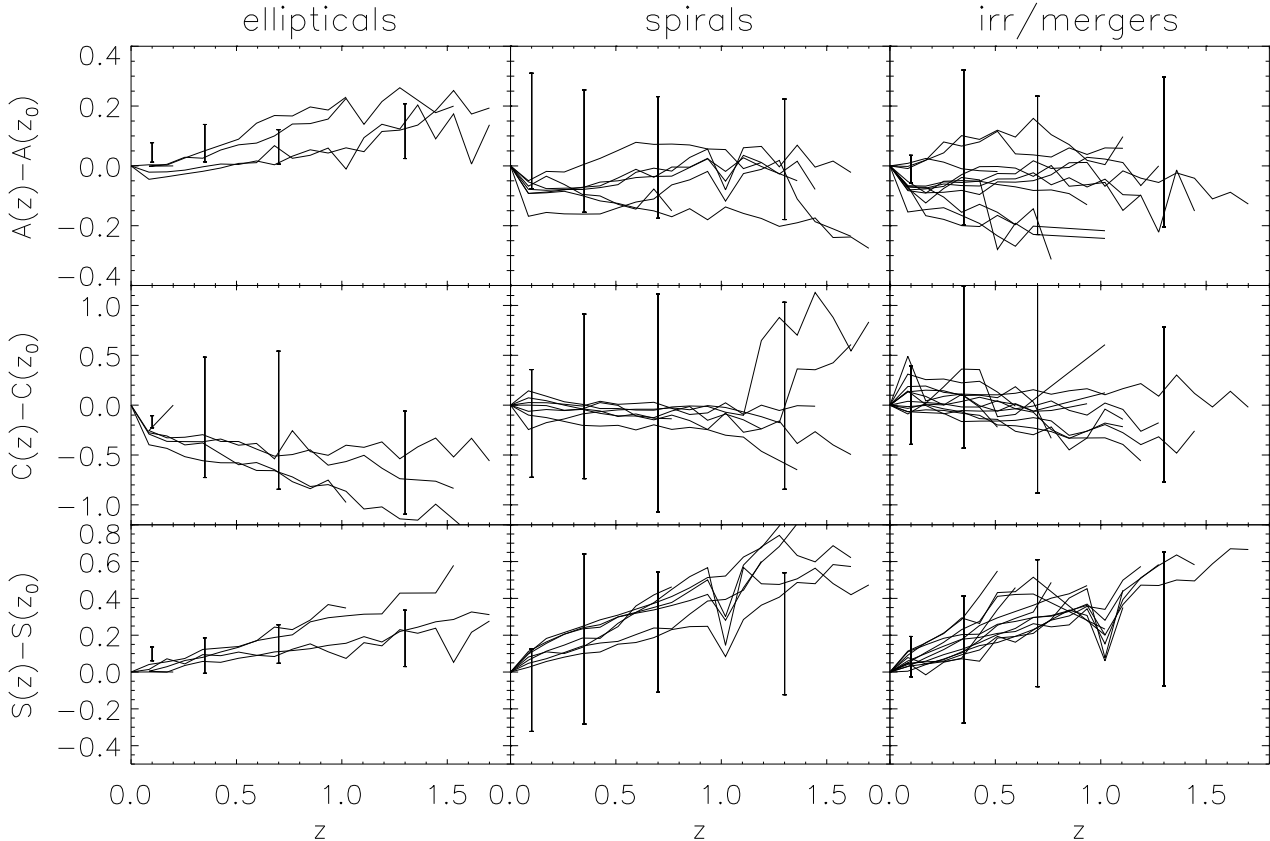


**Figure 6.** Evolution of the CAS parameters with  $z$  for a sample of artificially redshifted galaxies. 4 ellipticals, 7 spirals and 11 irregular galaxies are simulated at increasing redshift to isolate systematic effects. The resulting parameters for the entire sample in the four redshift bin is shown for comparison (vertical bars).

for all morphological classes, since the mean value increases artificially with redshift, while the scatter remains moderate.

Spirals and irregulars display a large spread in the values of the Concentration and Clumpiness which are not reproduced by our simulations, likely due to the small size of the local reference sample.

According to the measures of non-parametric indicators on real galaxies, up to redshift  $z \simeq 1.5$ , we have highlighted some biases in the CAS structure of galaxies, introduced by instrumental effects.

In conclusion, our simulations suggest that CAS parameters provide an effective tool to analyse and discriminate galaxy morphologies in the  $z$ -interval of the K20 sample.

#### 4.3.3 Results of the CAS analysis

Figures 7, 8 and 9 show the distribution of our galaxies sample in the CAS space in various redshift bins. The different symbols refer to our visual morphological classification as discussed in Sect. 4.1.

Objects in the morphological class 1 (ellipticals and S0s) separate significantly from the other classes. We have identified, independently from the redshift bin, the domains pop-

ulated mainly by early-type galaxies, which are bounded by the continuous lines in the figures. These boundaries are given by the following conditions:

$$A < 0.2, \quad C > 2.9, \quad 0.05 < S < 0.27 \quad A < 0.45 \times S + 0.085. \quad (5)$$

We stress that these boundaries are independent of the galaxy redshift. Only 1 elliptical galaxy lies outside from these regions (it is in fact a very small galaxy with an uncertain classification).

There are however 20 late-type galaxies out of 226 (9%), as judged from visual inspection, which fall within the early-type galaxy CAS domain, and so would be misclassified by such criterion. It is worth to note that using different boundaries for each redshift bin reduces the contamination of late-type in the ellipticals domain of a small amount. This contamination is due to the following objects: 8 galaxies dominated by a luminous and symmetric bulge, but with evidence for a faint disk; 3 ellipticals with a small companion in interaction; 5 very compact objects, for which CAS estimate is uncertain; 4 further symmetric and concentrated galaxies, but clearly patchy, for which the measure of the clumpiness essentially fails because of the small area and high ellipticity.

The datapoints corresponding to elliptical galaxies

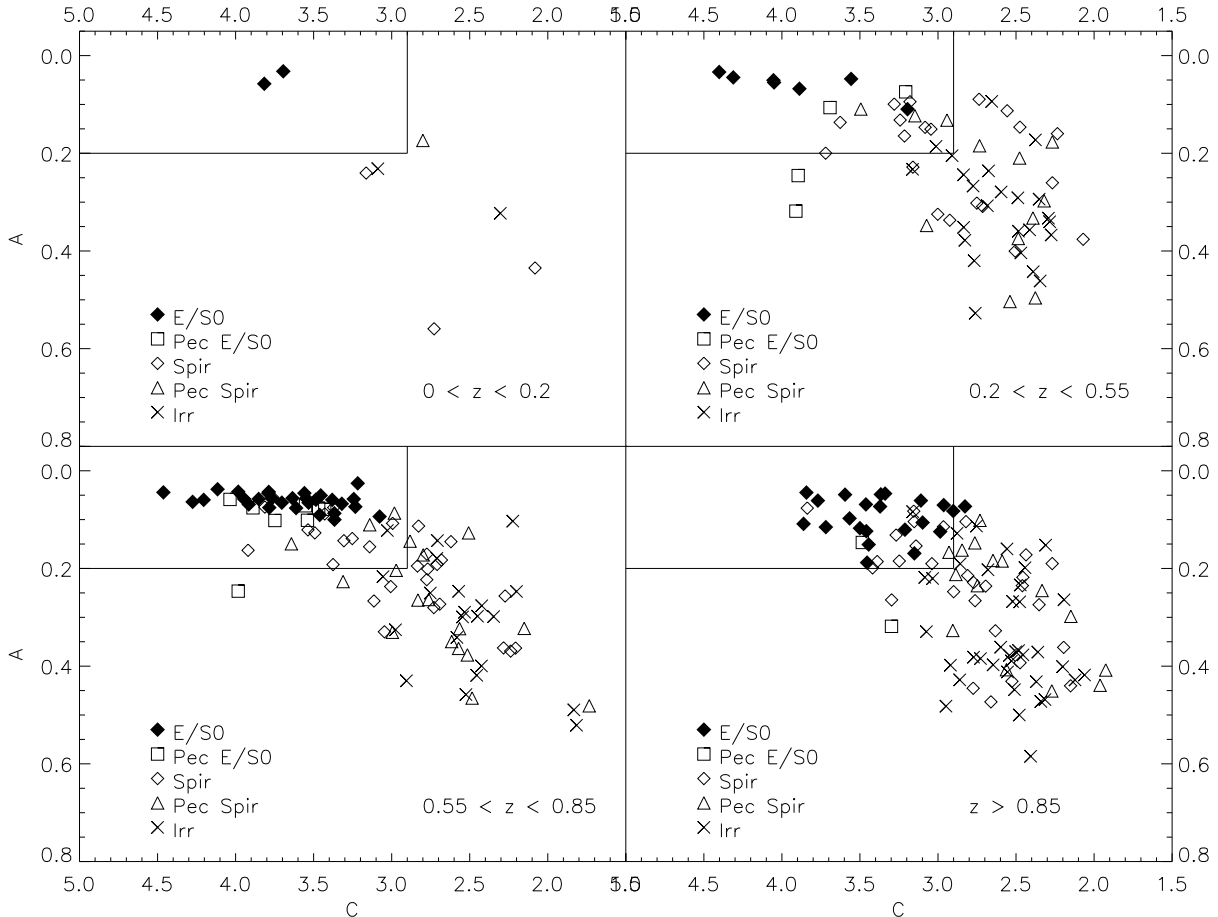


**Figure 7.** Evolution of the distribution of galaxies in the Concentration-Asymmetry plane in four redshift bins. The parameters are retrieved in the ACS band nearest to the B-rest frame: galaxies with  $z < 0.2$  are analyzed in the F435W filter, objects with  $0.2 < z < 0.55$  in the F606W filter, objects with  $0.55 < z < 0.85$  in the F775W filter and those with  $z > 0.85$  in the F850LP filter. The rectangle marks the region populated by ellipticals/S0 galaxies.

within the boundaries defined by eq.(5) show a scatter which sensibly depends on redshift: while it stays small up to  $z = 0.85$ , it tends to explode above this limit.

On the other hand, galaxies belonging to class 3, 4 and 5 do not show a tendency to segregate in the CAS plots, but they occupy almost the same regions.

In conclusion, the application of the CAS analysis to the K20 galaxies suggests this technique to be very efficient in disentangling early-type from late-type and irregular galaxies, with few percent of contamination. On the contrary, we failed in identifying algorithms able to resolve the different classes contributing to the late-type category.

#### 4.4 The Clumpiness-Asymmetry Relation for Galaxies

Conselice (2003) noticed that the Asymmetry and Clumpiness parameters for normal galaxies in the local universe are correlated, populating a strip in the S-A plane. On the other hand, merging systems or irregular galaxies have typically the same clumpiness of the interacting components

but higher asymmetry, hence they deviate from the relation. Fig. 10 confirms this trend in our sample: the two parameters are clearly correlated for normal ellipticals and normal spirals. Because of the different operative definitions of the CAS parameters with respect to those of Conselice (2003), we needed to recalibrate the relation. To this end we used the simulations described in Sect. 4.3.2 using data on 4 ellipticals and 3 normal spirals and changing their redshift: our simulated A-S relation for normal (E/Sp) galaxies is reported in the inset of Fig. 10, together with the strip containing the 90% of the data points. The best-fit relation and its 90% boundaries are:

$$A = (0.44 \pm 0.10)S + (0.08 \pm 0.08). \quad (6)$$

Fig. 10 reports the distribution of the galaxies in the S-A plane and the strip in which we expect to find only normal galaxies (defined as the strip that contain 90% of the simulated objects). The plot confirms that the large majority of visually inspected normal spirals and ellipticals fall indeed within the boundaries. Outside them only irregulars, peculiar spirals and some normal spiral are found.

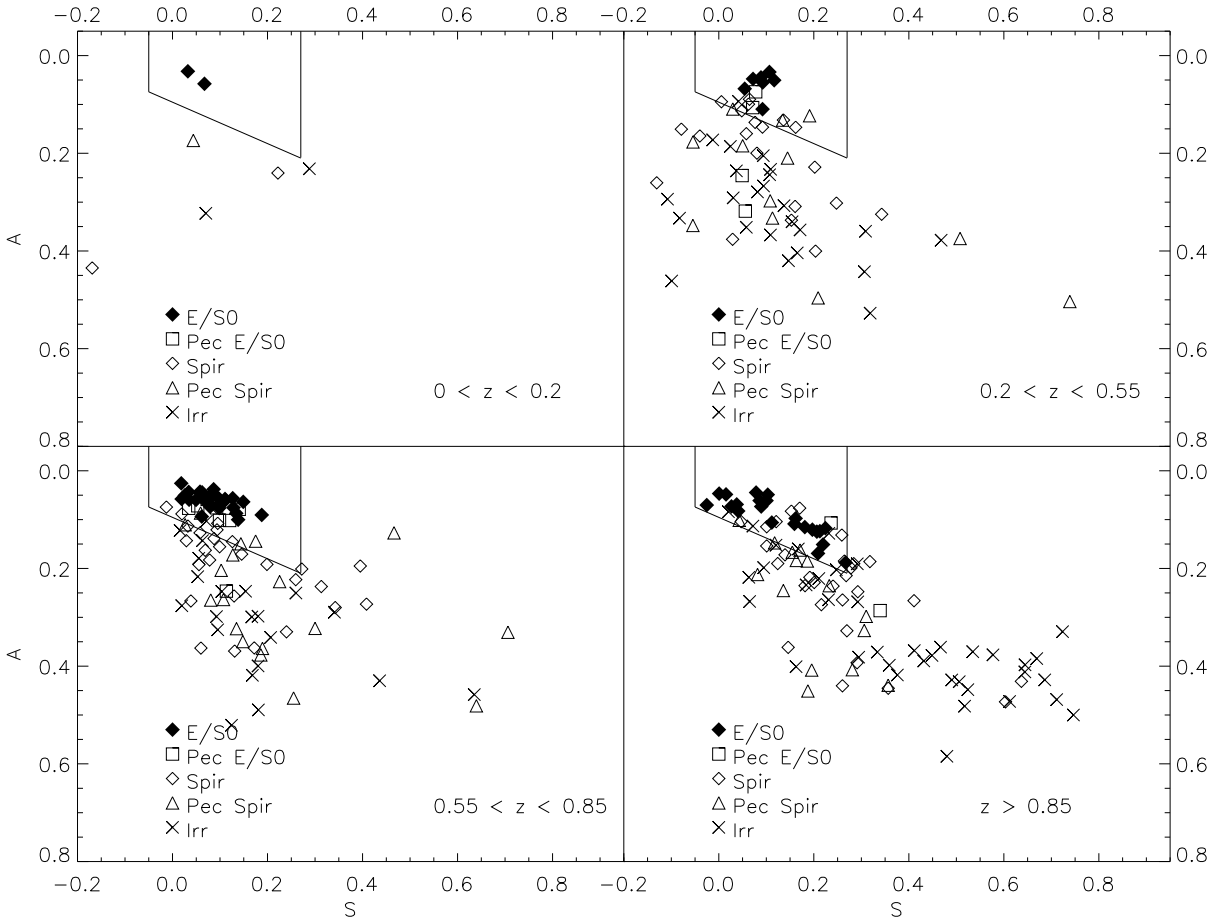


**Figure 8.** Evolution of the distribution of galaxies in the clumpiness-Asymmetry plane in four redshift bins. The parameters are retrieved in the ACS band nearest to the B-rest frame: galaxies with  $z < 0.2$  are analyzed in the F435W filter, objects with  $0.2 < z < 0.55$  in the F606W filter, objects with  $0.55 < z < 0.85$  in the F775W filter and those with  $z > 0.85$  in the F850LP filter. The lines marks the region typically populated by ellipticals/S0 galaxies.

However, this criterion appears of limited usefulness to disentangle normal spirals from irregulars because a large number of visually classified irregulars also fall in the normal galaxy region.

## 5 THE REDSHIFT DISTRIBUTIONS OF THE MORPHOLOGICAL CLASSES

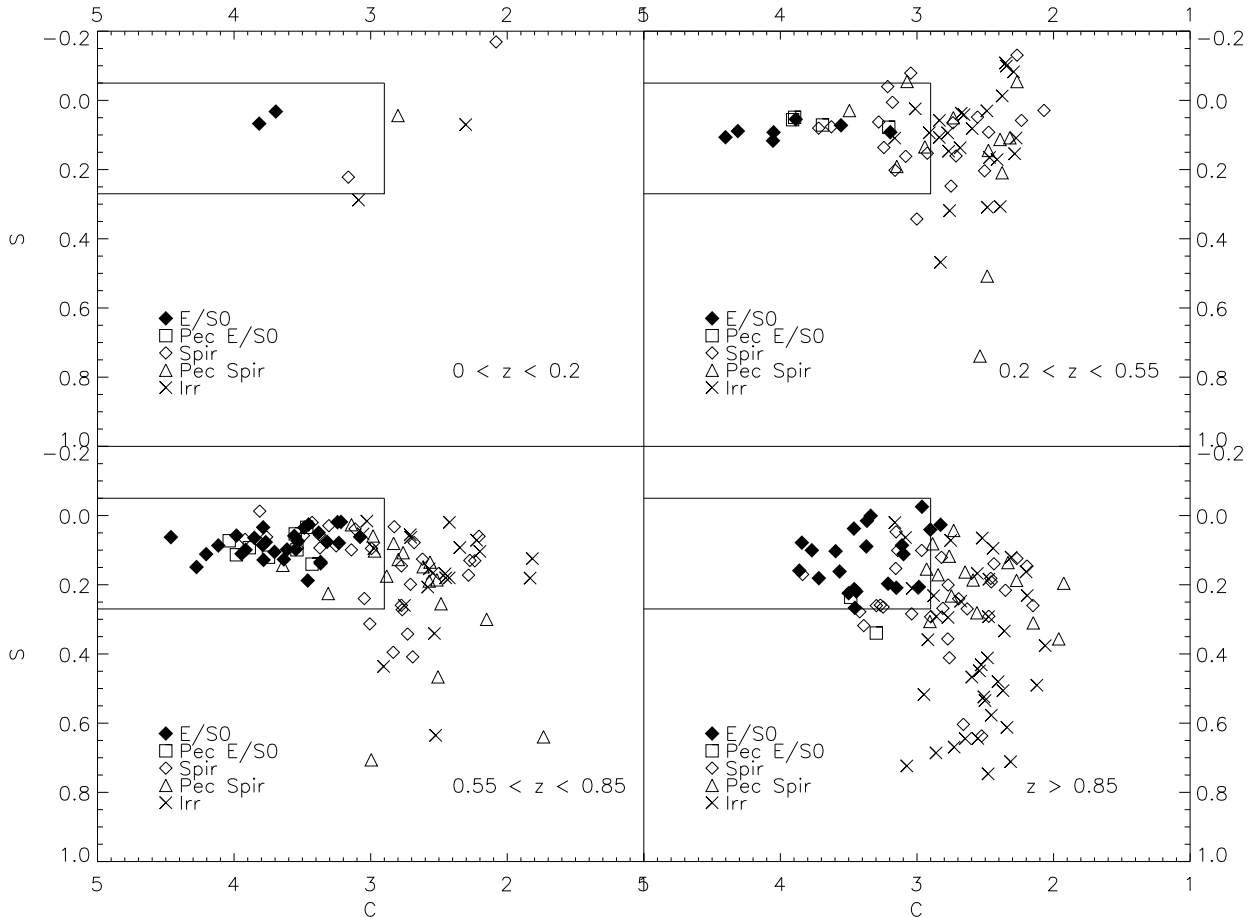
In Fig. 11 the redshift distribution for all the five morphological classes are reported. It should be noted the excess of early type galaxies and spirals at redshift  $z \sim 0.75$ , signature of the cluster of galaxies at  $\bar{z} = 0.737$ . The highest redshift elliptical is at  $z = 1.903$ . No disk galaxies lie at  $z > 1.8$ . Irregular galaxies instead are numerically relevant from  $z = 0.2$  up to  $z = 2.5$ .

Figure 12 shows the evolution of the fraction of morphological classes with the redshift. For clarity we used here only three main classes: early types (including type 1 and 2), disks (type 3 and 4) and irregular/peculiar (type 5). The shaded regions account for the effects of morphological  $K$ -

correction, as described in Sect. 4.1.1: the upper limit for the irregulars (and the lower for the spirals) corresponds to the (unrealistic) case in which the  $K$ -correction does not affect the classification of objects with  $z \gtrsim 1.2$ ; the lower limit for the irregulars (and the upper for the spirals) shows instead the case in which  $\sim 20\%$  of the morphologically classified irregulars at  $z \gtrsim 1.2$  are spirals.

The more evident result is the fast growth of the fraction of irregulars above  $z \sim 0.8$ , where they are the dominant population of the sample, being at  $z \gtrsim 1.5$  more than the 60% of the entire population. The Elliptical fraction remains near to 20% up to  $z = 1.5$  (beyond this redshift the statistic is too poor), except for the point at  $z \sim 0.75$ , where the fraction is higher due to presence of the two clusters. The fraction of disk galaxies remains rather constant to the 50% up to  $z \sim 1$ , then it decreases rapidly.

Conselice et al. (2004), studying the B-band rest-frame morphology of an I-selected sample of galaxies in the HDFs up to  $z=3$ , reach similar conclusions (see Fig. 9 therein): they also found a rapid decrease of ellipticals and spirals above  $z \sim 1$  and a contemporary increase in the number



**Figure 9.** Evolution of the distribution of galaxies in the Concentration-clumpinessSs plane in four redshift bins. The parameters are retrieved in the ACS band nearest to the B-rest frame: galaxies with  $z < 0.2$  are analyzed in the F435W filter, objects with  $0.2 < z < 0.55$  in the F606W filter, objects with  $0.55 < z < 0.85$  in the F775W filter and those with  $z > 0.85$  in the F850LP filter. The rectangle marks the region typically populated by ellipticals/S0 galaxies.

of peculiar galaxies. Our result however seems to be more robust at least up to  $z \sim 2$ : on the one hand, the K-band selection ensures a better mass sampling than the optical selection, and on the other hand, the larger area minimizes effects of cosmic variance. The accurate investigation of the effects of morphological  $K$ -correction conducted in previous sections avoids biases in the morphological fraction up to  $z \sim 2$ .

In Fig. 13 a comparison of the morphological fractions (early- and late-type only) obtained with various methods explored in this paper is proposed. In the top two panels the fractions of objects with  $n_{\text{Sersic}} \geq 2$  are shown against the redshift according to GASPHOT and GALFIT. In the bottom-left panel the early-type galaxies are selected according to their CAS parameters (see Eq. 5). Finally, in the bottom-right panel the results by the visual inspection are reported. Among the automatic methods, only the CAS parameters one is able to reproduce the results by the visual inspection. Among the  $\sim 250$  objects for which GASPHOT and GALFIT give acceptable fits,  $\sim 50\%$  have  $n_{\text{Sersic}} > 2$ . The late-type fraction obtained with the  $n_{\text{Sersic}}$  parame-

ter only suffers of two effects: the large number of irregular high asymmetric objects for which GASPHOT and GALFIT do not obtain an acceptable fit and the contamination of the Bulge dominated objects. The discrepancy between GASPHOT and GALFIT for objects with  $z \gtrsim 2$  (classified by the former as late and by the latter as early-type) must be considered rather marginal, due to the small number of galaxies in that redshift range for which GASPHOT and GALFIT found acceptable fits.

### 5.1 The Evolution of the Merging Fraction

The high resolution very deep imaging in the K20 field gives us also the opportunity to investigate the evolution of the merging fraction with the redshift for this K-band selected sample. Up to date, studies of the merging fraction against redshift have been done for optically selected (Patton et al. 1997, Le Fèvre et al. 2000) and NIR selected (Conselice et al. 2003) samples. In this paragraph, we investigate the evolutionary merging fraction using both pairs statistics (as i.e.

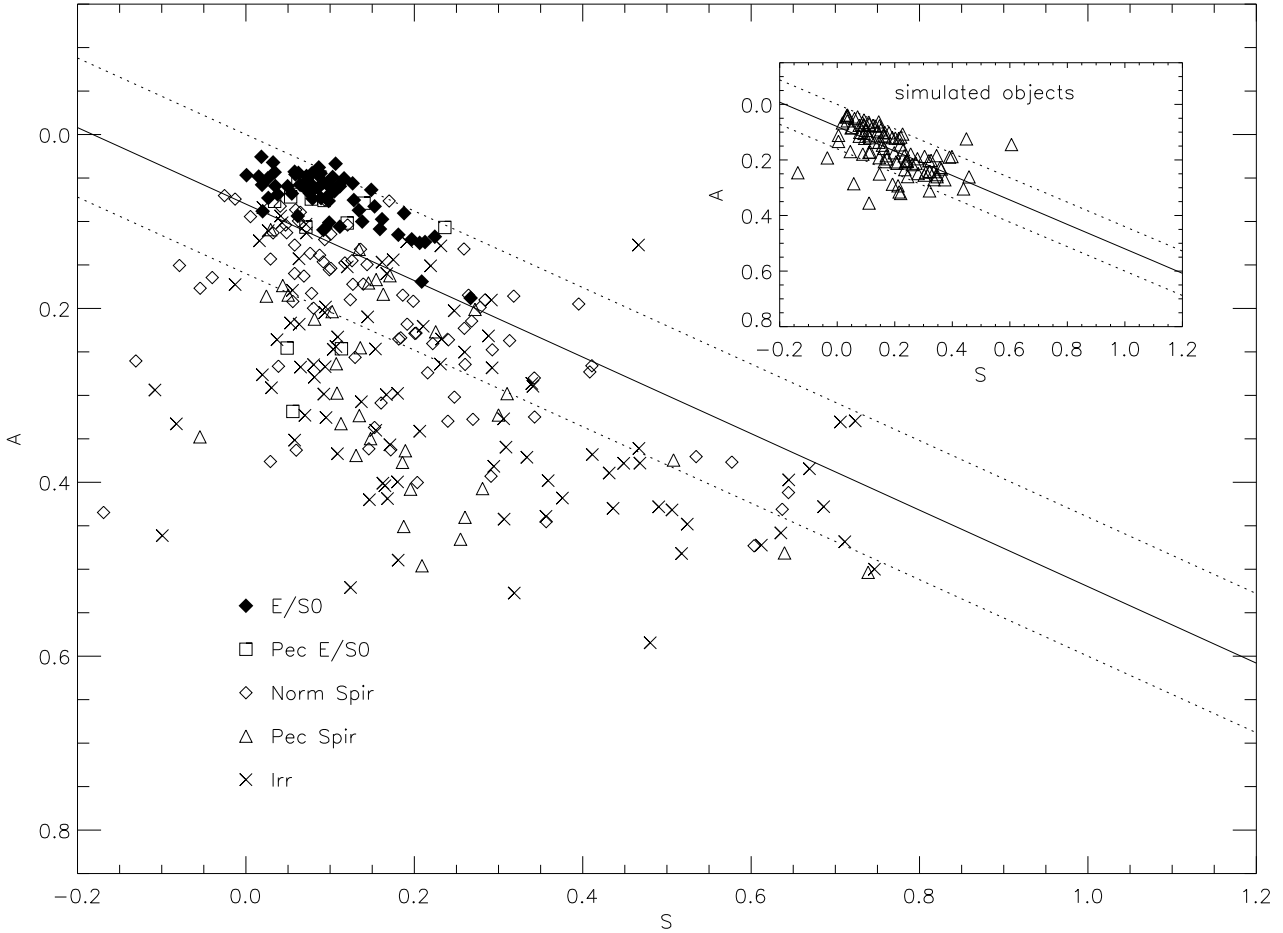


**Figure 10.** The distribution of the sample galaxies in the S-A plane. The strip between dotted lines shows the region containing normal galaxies, calibrated using the normal galaxies of the sample simulated at various redshifts, shown in the top-right panel.

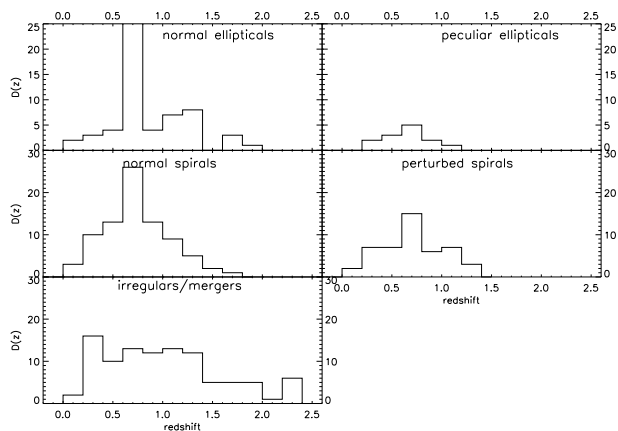


**Figure 11.** Redshift distributions for the five morphological classes.

Le Fèvre 2000) and asymmetry technique (Conselice et al. 2003).

Following Le Fèvre et al. (2000), we have visually identi-

fied in the K20 sample objects having a companion brighter than  $i=24.5$  within 20 kpc from the center, independently on the morphology of the main object, after removing cluster objects.

Given that in almost all cases we have the redshift only for the main object and we do not know if the observed pair consists of truly interacting objects or not. Then, we need to apply a correction factor accounting for this projection contamination. This correction is calculated integrating the galaxy number counts published by Driver et al. (1995) up to  $I=24.5$  within a circle of physical radius of 20 kpc. Given that at  $z < 0.5$  the 20 kpc radius projects over a large area, the high contamination of spurious pairs makes not statistically significant the measures at such low redshifts.

A second correction is needed to estimate how many of these physical pairs are going to merge. Here we use the correction proposed by Patton et al. (1997), suggesting that in the local universe half of the pairs with relative velocities less than  $350 \text{ km s}^{-1}$  are expected to merge within 0.5 Gyr. Given that the velocity is expected to vary with redshift as  $(1+z)^{-1}$ , the merging fraction is obtained by multiplying the pairs fraction (corrected for effects of projection) by  $0.5(1+z)$ .

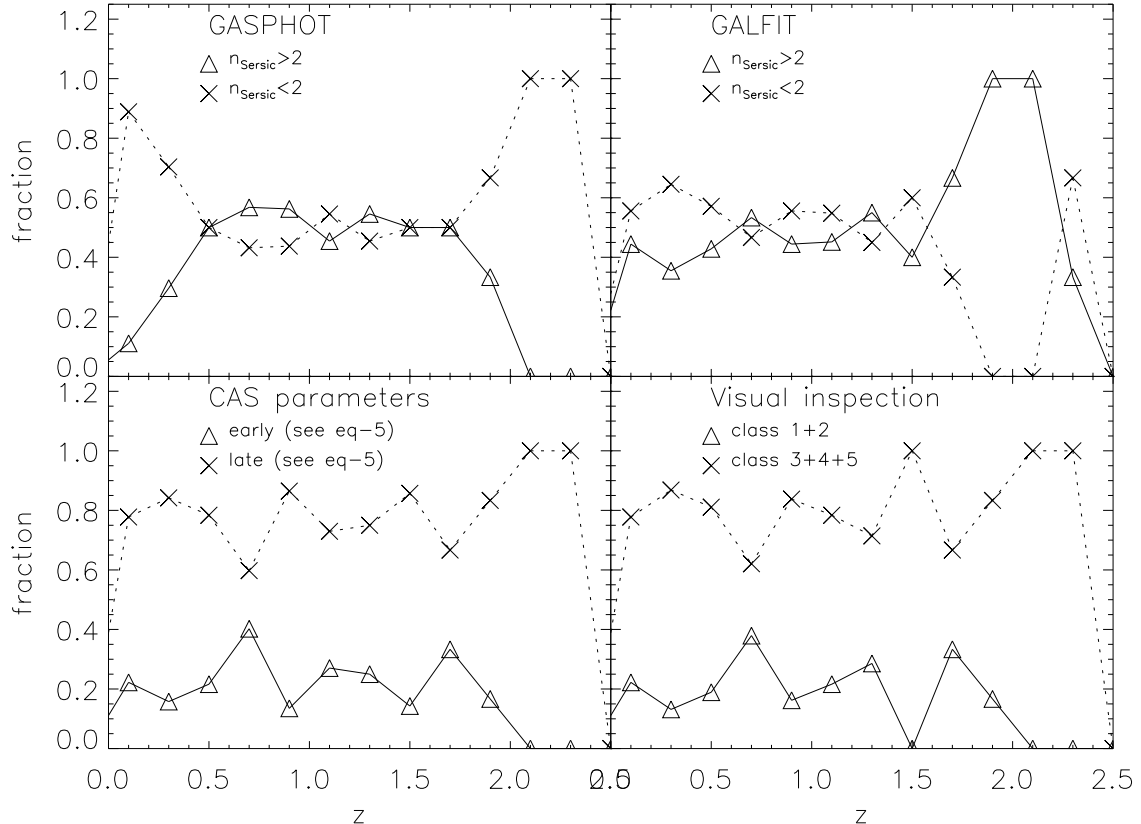


**Figure 13.** Morphological fractions for early- and late-type galaxies as a function of the redshift obtained by the different methods proposed in this paper: in the top two panels the criterion based on  $n_{\text{Sersic}} \gtrless 2$  is used for GASPHOT and GALFIT; in the bottom-left panel early-galaxies are selected according to Eq. 5; in the bottom-right panel the visual classification is used.

For comparison, we have recomputed the merging fraction in a completely different way, based on asymmetry computation (Conselice et al. 2003): an object is identified as merger if it has an asymmetry greater than a certain value (in this case  $A > 0.4$ ). Also in this case cluster objects have been removed. This technique selects a different class of objects compared with those identified by pairs statistics. Given that it is computed in a small area around the object, the highest asymmetry is measured for strongly interacting objects, rather than for objects in a pair often separated by many kiloparsecs, and that therefore do not fall together in the area for the asymmetry computation. Moreover, the merging fraction obtained by the asymmetry technique strongly depends on the border value of  $A$  used for merger identification.

Figure 14 reports the inferred merging fraction for the K20 sample as a function of the redshift both from pair statistic (filled circles) and from asymmetry criterion (filled squares). The results from the two techniques are in good agreement with each other, and with those obtained by other authors. Our data, together with those by Le Fèvre et al. (2000), Patton et al. (1997) and Conselice et al. (2003) provide the evolution of the merging fraction as  $a(1+z)^m$ , where

$a$  and  $m$  are free parameters:

$$f_{\text{merg}} = (0.022 \pm 0.002) (1+z)^{2.2 \pm 0.3}. \quad (7)$$

The value of  $m$  is in quite good agreement with  $m = 2.8 \pm 0.9$  obtained by Patton et al. (1997) using only its data at  $z < 0.3$ , but is smaller than the value obtained by Le Fèvre et al. 2000 ( $m = 3.4 \pm 0.6$ ). We can conclude that the fraction of merging evaluated for a K-band selected sample increases up to  $z \sim 1.5$ , according with previous works, but, due to the limited statistic, we can not constrain the evolution for higher redshift. There are however indications that it remains lower than 20% up to  $z=2$ .

It must be noted that if it is true that the asymmetry and pairs techniques select different merging events (observed respectively in late and early phases), the merging fraction could be the sum of the two, then the numbers in Fig. 14 must be multiplied by a factor 2.

## 6 COMPARING THE MORPHOLOGICAL AND SPECTROSCOPIC CLASSIFICATION

In Table 1 we report a comparison between morphological and spectroscopic classifications for our sample galaxies.

spectral class	ell.	perturbed ellipticals	normal spirals	perturbed spirals	irr/mer	all types
Early type	51	5	6	3	1	66
Early+EmLines	5	3	20	3	7	38
Emission lines	2	6	53	41	76	178
Unobs./Unid.	2	0	1	1	14	18
Total	60	14	80	48	98	300

**Table 1.** Comparison between morphological and spectroscopical classification.

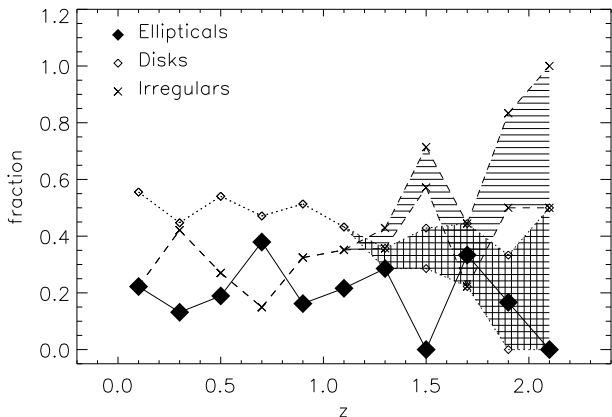


**Figure 12.** Morphological fractions as a function of the redshift. The results for  $z \gtrsim 1.2$  are likely to be affected by morphological  $K$ -correction, given that at those redshifts z-band does not match more the B rest-frame, but the U rest-frame. We showed in Sect. 4.1.1 that the  $\sim 20\%$  of the galaxies with  $z \sim 1$  classified as spirals in their B rest-frame appear as irregulars in their U rest-frame. The shaded regions show the confidence interval for irregulars and spirals galaxies. The datapoint at  $z=0.7$  is affected by the presence of the two clusters.

The two classifications have been made completely independently.

Among the 18 spectroscopically unobserved or unidentified objects, 15 fall in the irregular class. The bulk of them (9/15) are low surface brightness objects very close to the optical detection limits. For the remaining object with both spectroscopic and morphological classification, the agreement is quite good: 51/60 normal ellipticals have an early type spectrum, 118/128 spirals (morphological class 3 and 4) and 97/98 irregulars have late type or early+emission-line spectra.

Among the galaxies classified as normal ellipticals, there are 5 objects with early spectra, but showing some emission lines, and 2 galaxies with emission lines spectra. Among these 7 objects, 4 are small and with difficult morphological classification (Sérsic indices  $n > 2.3$  and  $r_e < 0.25''$ ); one has been classified as S0/Sa, because of the axial ratio near to 0.5, even if a clear disk component is not so evident; the remaining 2 have clearly an elliptical morphology ( $n > 4$ ).

Among the 14 galaxies that we have morphologically classified as peculiar ellipticals (galaxies with a dominant

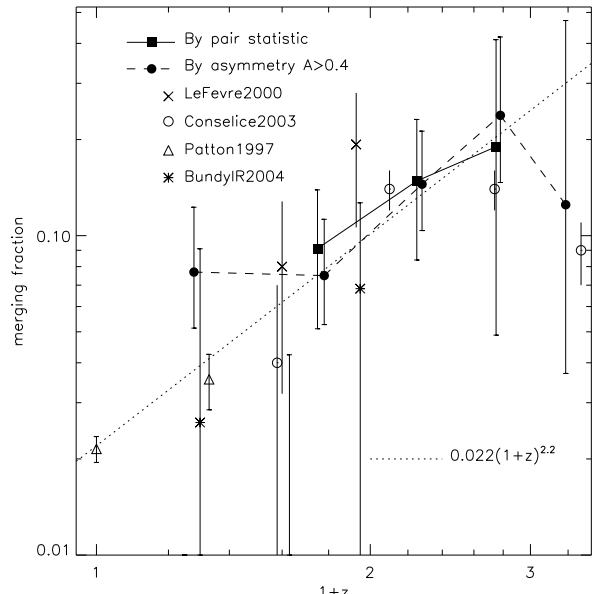


**Figure 14.** The inferred merging fraction for the K20 sample as a function of the redshift, both from pairs statistics (filled circles) and from asymmetry criterion (filled squares). Errors bar are calculated by a Poisson statistic. Results of previous works are also reported, together with the best-fit relation to the data (dotted line).

elliptical component, but with signs for distortion of the isophotes), 9 have emission lines in their spectrum, showing that a certain degree of activity is really present in the galaxies. In this morphological class however 5 galaxies that show no signs of emission lines fall.

Ten late-type galaxies (belonging to the morphological classes 3, 4 and 5) show early-type spectra with no signs for emission lines. In 6 cases a luminous and concentrated bulge dominates the spectrum, probably overwhelming the contributions from the star-forming regions. In one case the classification is uncertain due to the small area covered by the galaxy. The agreement between morphological and spectroscopic properties is good also for the galaxies belonging to the two clusters: only 1 object classified as elliptical shows signs of emission lines, whereas 4 late-type galaxies have early-type spectra.

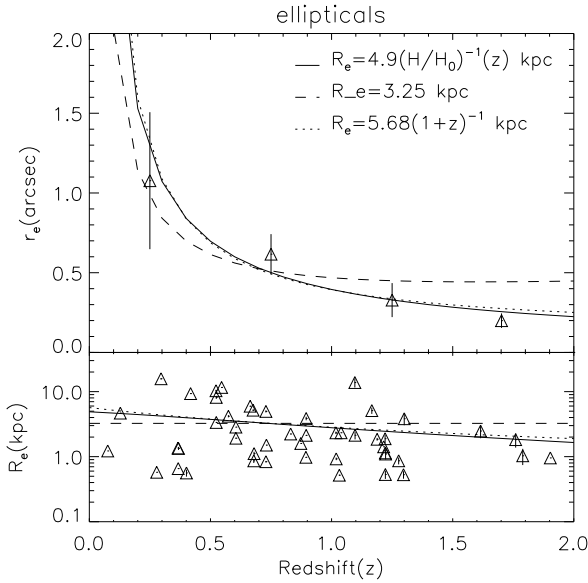


**Figure 15.** The evolution with the redshift of the galaxy sizes of elliptical class. *Upper panel*: mean angular size in four redshift bins compared with three models of evolution for the physical galaxy size. For each point error bars represent the standard deviation divided by the square root of the number of galaxies in that bin. Continuous and dotted lines are two model in which galaxy size evolves with the redshift respectively as  $(H/H_0)^{-1}$  and as  $(1+z)^{-1}$ , whereas dashed line is a model of constant size. The three curves are normalized to the observed mean value at redshift  $0.5 < z < 1$ . *Lower panel*: the physical sizes of early type galaxies are reported as a function of the redshift. The three models of evolution and no-evolution of galaxy sizes are also reported.

## 7 GALAXY SIZES VERSUS REDSHIFT

A critical prediction of galaxy formation models concerns the evolution of the physical sizes. The disk scale-lengths, in particular, are predicted to decrease proportionally to the inverse of the Hubble parameter (Fall & Efstathiou 1980). We have investigated the evolution with the redshift of the galaxy sizes for early/type (class 1 and 2), disks (class 3 and 4) and irregulars (class 5) up to  $z \sim 1.5$ .

As a measure of the physical size of galaxies we use the effective radius  $r_e$  retrieved by GASPHOT by fitting the galaxy light profile with a Sérsic model.

In the upper panels of Figs. 15, 16 and 17 we report the mean angular size in four redshift bins ( $z < 0.5$ ,  $0.5 < z < 1$ ,  $1 < z < 1.5$  and  $z > 1.5$ ) respectively for ellipticals, spirals and irregulars. Cluster galaxies can be recognized at  $\bar{z} = 0.736$  and  $\bar{z} = 0.668$ .

For comparison, the curves corresponding to no-evolution of the physical size, evolution with the inverse of Hubble parameter  $H(t)$  and evolution with  $(1+z)^{-1}$  are also plotted, each normalized to the observed datapoint at  $z = 0.75$ . In the lower panels, the data on the physical sizes for individual galaxies are reported.

Our results do not show much evidence for size evolution in the explored redshift range. In particular, spirals and irregulars are entirely consistent with no evolution, in good agreement with the results of Ravindranath et al. (2004),

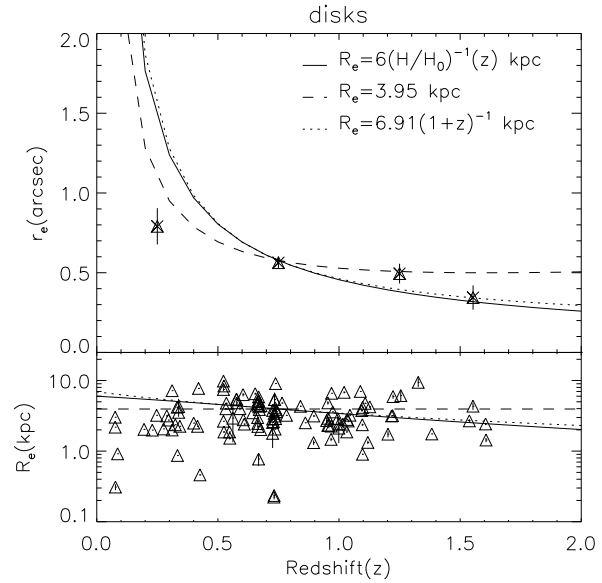


**Figure 16.** Same as Fig. 15 for disk galaxies.

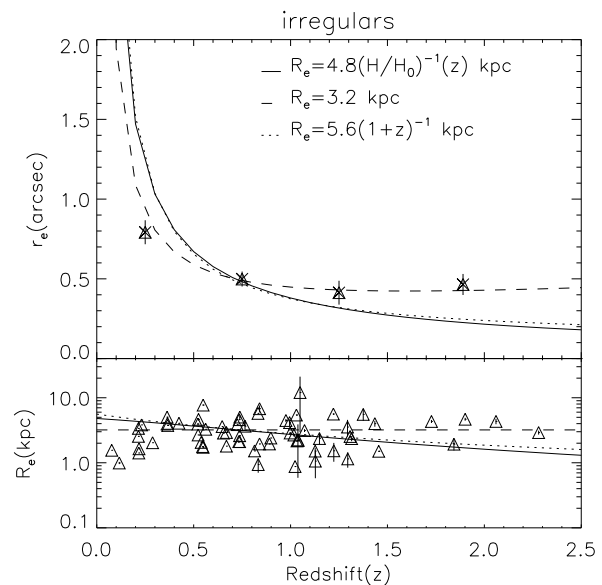


**Figure 17.** Same as Fig. 15 for irregular galaxies.

who payed particular attention in discussing the observational biases.

A small decrease of  $R_e$  may be seen for the elliptical population, for which our results are consistent with  $R_e \propto (H/H_0)^{-1}$ . The statistical significance of this result is however not at all marginal: we point out that at high  $z$ ,  $K$ -band selects only the most massive and luminous galaxies, while at low  $z$  the explored mass interval is much more wide.

## 8 DISCUSSION AND CONCLUSIONS

We have exploited very deep and high resolution ACS/HST imaging recently become available in the CDFS area and covering a major portion of the K20 survey, to conduct an accurate morphological analysis of the K20 sample high-redshift galaxies. For each object, the analysis has been performed in the ACS band closer to the B-band rest-frame in order to minimize effects of morphological  $K$ -correction.

Our main results are hereafter summarized.

(i) From visual classification (performed by three authors), we find that: 60 galaxies are normal ellipticals or S0; 14 are peculiar ellipticals; 80 are normal spirals; 48 spirals showing signs of interaction or of regions of excess star formation; 98 are irregular galaxies. We have carefully investigated the effects of the morphological  $K$ -correction on the objects at  $z \gtrsim 1.2$ , for which the B-band rest-frame is not available, establishing robust upper and lower limits to the fraction of each morphological class.

(ii) We have investigated the capabilities of parametric and non-parametric techniques in disentangling morphological classes with a low level of interaction. In particular, we used the GALFIT and GASPHOT packages to fit the light distribution with the Sérsic parametric model, to exploit the correlation between Sérsic indices and B/D ratios.

We have shown that parametric tools like GASPHOT and GALFIT are not completely efficient in distinguishing between early- and late-type objects. They do not find acceptable fits for  $\sim 50/300$  objects, mainly those with high asymmetry or low surface brightness. The general agreement of these two tools for the remaining objects is quite good (while for  $\sim 10\%$  they turn out to be completely inconsistent). The agreement worsens at increased asymmetry of the objects, as expected (see Figs. 3 and 5). The distributions of the Sérsic indices for the different visual morphological classes turn out to be quite similar for the two tools (see Fig. 4). It is interesting to note that a quite substantial number ( $\sim 50/250$ ) of visually classified late-type galaxies have a high Sérsic index ( $n > 2$ ): this case may be produced by a prominent bulge on top of a tiny disk structure.

(iii) We have complemented the morphological analysis with the calculation of non-parametric quantities like Concentration, Asymmetry and Clumpiness for the objects in the sample. We have shown that there is a precise region of the CAS space (defined by Eq. 5) occupied mostly by early type galaxies: ellipticals are the objects with higher Concentration and smaller Clumpiness and Asymmetry. Only one elliptical falls out, while 20 late type lie within this region.

Simulations have been performed to investigate the reliability of the CAS values retrieved at high redshifts. It has been shown that some biases in the measures are introduced by the degradation of the resolution at high  $z$ , somehow preventing an assessment of the intrinsic evolution of the CAS parameters.

(iv) We have shown that a criterion based on the Sérsic index only does not completely segregate early- by late-type galaxies (see Fig. 13; we have already mentioned the many low surface brightness or highly asymmetric objects for which the fit procedures do not converge, and the number of late-type galaxies with a Sérsic index  $n_{\text{Sersic}} > 2$ ).

The CAS criterion instead better reproduces the classifi-

cation between early- and late-type obtained by visual inspection (see Fig. 13).

(v) Over the 300 objects of the sample, only 74 turn out to be early type galaxies (our class 1 and 2). Their redshift distribution is dominated by the cluster at  $z \sim 0.737$ , and the number decreases rapidly for  $z > 1.5$  following the general trend for a rapid decrease at such  $z$  for the whole population.

The most numerous galaxies are the irregulars: 1/3 of the objects in the sample belongs this class. Their fraction increases from  $\sim 20\%$  at low- $z$  to  $\sim 60\%$  at  $z > 1.2$  and is dominant at higher redshifts. The simultaneous decrease of early and disk galaxies suggests intuitively that some amounts of high redshift irregular galaxies may progressively transform into the local elliptical and spiral galaxy population. A conclusion on this important issue would however require much improved statistics in the critical redshift interval of  $z \sim 1.5$  to 2. In any case our analysis indicates a predominance of spirals and irregulars in K-band selected samples at even moderate depths.

We stress that these results turn out to be rather robust, thanks to the use of the B-band rest-frame up to  $z \sim 1.2$ , (so minimizing effects of morphological  $K$ -correction), and to the accurate assessment of biases introduced by the  $K$ -correction at higher  $z$ .

(vi) We also analyse the evolution with the redshift of the merging fraction. We use both the pair statistics technique and the asymmetry criterion  $A > 0.4$ , in order to measure merging fraction. Although the two techniques likely select two different kinds of objects (corresponding to early and late phases of a merger), we found that the results of each criterion are in good agreement with each other and with previous works. The inferred merging fraction remains in any case lower than 20% up to  $z = 2$ . If we consider that the total merging fraction is the sum of the two, then the numbers in Fig. 14 are to be multiplied by a factor  $\sim 2$ .

(vii) We have performed a systematic comparison between morphological and spectroscopic classification, showing quite good agreement: 91% of the sample have spectral characteristic compatible with morphological ones. There are some ellipticals (7/60) with a very relaxed morphology showing emission lines in their spectra. The late-type objects showing early-type passive spectra are mainly bulge-dominated spirals, for which probably the signal from the disk component is overwhelmed by the concentrated and luminous bulge.

(viii) Finally the redshift dependence of galaxy sizes is investigated for elliptical (class 1+2), disk (class 3+4) and irregular (class 5) galaxies separately. Our results show no evolution for the sizes of disks and irregulars, whereas a small decrease of  $R_e$  has been found for elliptical galaxies: their sizes seems to vary as  $R_e \propto (H/H_0)^{-1}$ . These results are particularly important if we consider that we are selecting at the high redshifts the most luminous, massive, hence the largest, of the galaxy population at that cosmic epoch.

**ACNOWLEDGEMENTS:** We are grateful to the referee, Roberto Abraham, for careful reading and interesting comments on the manuscript.

REFERENCES

Abraham, R. G., Tanvir, N. R., Santiago B. X. et al., 1996, *MNRAS*, **279**, 47

Abraham, C., 1998, IAU Symp. 186, Galaxy Interactions at Low and High Redshift, astro-ph/9802033

Bertin, E. and Arnouts, S., 1996, *A&AS*, **117**, 393

Bundy, K., Fukugita, M., Ellis, R. S. et al., 2004, *ApJ*, **601**, L123

Caon, N., Capaccioli, M. and D'Onofrio, M., 1993, *MNRAS*, **265**, 1013

Cimatti, A., Mignoli, M., Daddi, E., et al., 2002, *A&A*, **392**, 395

Cimatti, A., Pozzetti, L., Mignoli, M., et al., 2002, *A&A*, **391**, 1L

Cimatti, A., Daddi, E., Cassata, P., et al., 2003, *A&A*, **412**, 1L

Cimatti, A., Daddi, E., Renzini, A., et al., 2004, *Nature*, **430**, 184

Conselice, C., Bershady, M. and Jangren, A., 2000, *ApJ*, **529**, 886

Conselice, C., 2003, *ApJS*, **147**, 1

Conselice, C., Bershady, M., Dickinson, M. and Papovich, C., 2003, *AJ*, **126**, 1183

Conselice, C., Blackburne J. A. and Papovich, C., 2004, astro-ph/0405001

Daddi, E., Cimatti A., Renzini, A., et al., 2004, *ApJ*, **600**, 127L

Driver, S. P., Windhorst, R. A., Ostander, E. J. et al., 1995, *ApJ*, **449**, L23

Fall, S. M. and Efstathiou, G., 1980, *MNRAS*, **193**, 189

Giavalisco, M., Ferguson, H. C., Koekemoer, A. M. et al., R., 2004, *ApJ*, **600**, L93

Glazebrook, K., Ellis, R., Santiago, B. and Griffiths, R., 1995, *MNRAS*, **275**, L19

Le Fèvre, O., Abraham, R., Lilly, R. S. et al., 2000, *MNRAS*, **311**, 565

Marzke, R. O., Da Costa, L. N., Pellegrini, P. S. et al., 1998, *ApJ*, **503**, 617

Mignoli, M., et al., 2004, in prep.

Patton, D. R., Pritchett, C. L., Yee, H. K. C. et al., 1997 *ApJ*, **475**, 29

Papovich, C., Giavalisco, M., Dickinson, M. et al., 2003 *ApJ*, **598**, 827

Peng, C. Y., Ho, L. C., Impey, C. D., Rix, H., 2002 *AJ*, **124**, 266

Pignatelli, E., Fasano, G. and Cassata, P., 2004, submitted

Ravindranath, S., Ferguson, H. C., Conselice, C. et al., 2004, *ApJ*, **604**, L9

Simard, L., Willmer, C. N., Vogt, N. P. et al., 2002, *ApJS*, **142**, 1

van den Bergh, S., Cohen, J. G., Hogg, D. W. and Blandford, R., 2000, *AJ*, **120**, 2190

van den Bergh, S., Cohen, J. G. and Crabbe, C., 2001, *AJ*, **122**, 611

Vanzella, E., Cristiani, S., Dickinson, M. et al., 2004, astro-ph/0406591

Windhorst, R. A., Taylor, V. A., Jansen, R. A. et al., 2002, *ApJS*, **143**, 113